Materials Transactions, JIM, Vol. 41, No. 11 (2000) pp. 1423 to 1426
Special Issue on Bulk Amorphous, Nano-Crystalline and Nano-Quasicrystalline Alloys

Glass Forming Ability and Properties of Zr/Nb-Based Bulk Metallic Glasses

Yong Zhang, De Qian Zhao, Ru Ju Wang, Ming Xiang Pan and Wei Hua Wang*

Institute of Physics & Center for Condensed Matter Physics, Chinese Academy of Sciences, Beijing 100080, P.R.China

Zr/Nb-based bulk metallic glasses (BMGs) with excellent glass forming ability (GFA) and high thermal stability were obtained by water quenching method. The GFA of the alloys is sensitive to the Fe addition, and the highest GFA is achieved at 8 at% of Fe addition. It is found that ΔT defined by the difference between the onset temperature of the first crystallization event T_x and the glass transition temperature T_g ($\Delta T = T_x - T_g$) is more effective than T_{rg} ($T_{rg} = T_g/T_m$, T_m, melting temperature) to reflect the GFA of the Zr/Nb-based BMGs. The elastic properties of the alloys are investigated by ultrasonic measurements.

(Received May 15, 2000; Accepted July 24, 2000)

Keywords: *bulk metallic glasses, glass-forming ability, ultrasonic measurements*

1. Introduction

Recently, multicomponent bulk metallic glasses (BMGs) with excellent glass forming ability (GFA) were developed in a variety of systems such as La–Al–Ni, Mg–Cu–Y, Pd–Ni–Cu–P, Zr–Ti–Cu–Ni–Be, Zr–Al–Ni–Cu–Ti, Fe–Cr–Mo–Ga–P–C–B, and Nd–Fe–Al.[1–5] The BMGs can be produced at a lower cooling rate of 1 $\sim$ 100 K/s. For conventional metallic glasses, they can only be obtained at a very high cooling rate of 10^5 $\sim$ 10^6 K/s[6] which limits their shapes to be thin ribbons, wires and droplets. The BMG can be forged in the supercooled liquid region (SLR) (defined as the difference between the glass transition temperature T_g and the onset crystallization temperature T_x, $\Delta T = T_x - T_g$) into different types of shapes.[4] With the bulk shapes, many property measurements, such as tensile test and the ultrasonic measurement can be processed easily and precisely. Another attractive characteristic of the BMG is the unique properties, such as excellent soft magnetism, high corrosion resistance, excellent elastic and mechanical property.[2] Zr–Ti–Cu–Ni–Be is a well studied BMG system so far, its critical cooling rate is lower than 1 K/s.[7] The previous studies[8] show that 2 $\sim$ 8 at%Fe addition does not obviously change the GFA of the Zr/Ti-based BMG, however, 10 $\sim$ 18 at%Fe addition significantly reduces the GFA, and nanocrystalline composite is obtained, the average diameter of nanocrystalline grains is about 5 nm. Zr–Nb–Cu–Ni–Be is another BMG system with excellent GFA reported in Ref. 9), the BMG exhibits high values of T_g, T_x and T_m, meaning high thermal stability and wide application temperature region. In this paper, the GFA, thermal and elastic properties of Zr/Nb-based BMG are investigated. The different effects of Fe addition on the GFA comparing to that of the Zr/Ti-based BMG are found. The elastic properties of the alloys are investigated by ultrasonic measurements.

2. Experimental Procedure

Ingots of the alloys were prepared by arc melting a mixture of constituent elements in argon atmosphere, the compositions of the alloys are listed in Table 1. The ingots were remelted in a vacuum-sealed quartz tube and quenched in water. The sample rods with diameter of 3 $\sim$ 8 mm were cut into 10 mm-long cylinders and 0.5 mm-thick slices. The cylinders were used for the ultrasonic measurements, and the slices were used for X-ray diffraction (XRD) analysis, differential temperature analysis (DTA), transmission electron microscope (TEM) observation, and hardness measurement. XRD was using a Siemens D5000 X-ray diffractometer with Cu K_α radiation. DTA and DSC measurements were performed in Perkin Elmer DTA-7 and DSC-7 with a heating rate of 0.33 K/s. The density was measured by Archimedean method. The Vickers hardness (H_V) was measured by Microhardness-71 at a load of 200 g. Ultrasonic velocities were measured using a pulse echo overlap method. The travel time of the ultrasonic waves propagating through the sample was measured using a MATEC 6600 ultrasonic system with a measuring sensitivity of 0.5 ns. The carrying frequency was 10 MHz. Composition of the alloys was determined by chemical analysis. The isothermal annealing was performed in a

Table 1 The compositions, structures and sizes of the ZrNbCuNiFeBe alloys.

Alloys	Alloy composition	diameter	Structure
A1	$Zr_{41}Nb_{14}Cu_{12.5}Ni_8Be_{22.5}Fe_2$	8 mm	c
A2	$Zr_{41}Nb_{14}Cu_{12.5}Ni_5Be_{22.5}Fe_5$	8 mm	c
A3	$Zr_{41}Nb_{14}Cu_{12.5}Ni_2Be_{22.5}Fe_8$	8 mm	a + c
B0	$Zr_{45}Nb_{10}Cu_{13}Ni_{10}Be_{22}$	3 mm	a
B1	$Zr_{45}Nb_{10}Cu_{13}Ni_8Be_{22}Fe_2$	8 mm	c
B2	$Zr_{45}Nb_{10}Cu_{13}Ni_5Be_{22}Fe_5$	8 mm	c
B3	$Zr_{45}Nb_{10}Cu_{13}Ni_2Be_{22}Fe_8$	8 mm	a + c
B4	$Zr_{45}Nb_{10}Cu_{13}Be_{22}Fe_{10}$	8 mm	a + c
B5	$Zr_{45}Nb_{10}Cu_{13}Be_{17}Fe_{15}$	8 mm	a + c
C0	$Zr_{48}Nb_8Cu_{14}Ni_{12}Be_{18}$	8 mm	a
C1	$Zr_{45}Nb_8Cu_{13}Ni_4Be_{22}Fe_8$	5 mm	a
C2	$Zr_{45}Nb_8Cu_{13}Ni_2Be_{22}Fe_{10}$	8 mm	a + c
C3	$Zr_{48}Nb_8Cu_{12}Fe_8Be_{24}$	8 mm	a

In the structure column, "a" represents amorphous state and "c" represents crystalline state.

*Corresponding author, E-mail: whw@aphy.iphy.ac.cn

vacuum furnace (10^{-3} Pa). To ensure the same thermal history for all samples, each sample was heated up using a rate of 0.17 K/s and cooled with the rate of 0.17 K/s back to room temperature.

3. Results and Discussion

Figure 1 shows DTA curves of six Zr/Nb-based alloys with higher GFA optimized from a series of experiments, each of the alloys shows a glass transition process, which is a common feature in almost all BMGs. The crystallization of the alloys C0 [Fig. 1(a)] and B0 [Fig. 1(b)] exhibits two step process; a main process follows with a small one, the second crystallization temperature decreases with increasing Nb content from 8 at% to 10 at%. With Fe addition, the crystallization processes exhibit three steps for the alloy B3 [Fig. 1(c)], C1 [Fig. 1(d)] and A3 [Fig. 1(e)], and four steps for the alloy B4 [Fig. 1(f)]. This means, with more Fe addition, the crystallization process is getting more complicated. Figs. 1(a) and (b) show a single melting process meaning that the compositions of the two alloys are in eutectic point. Figs. 1(c), (d), (e) and (f) show a two-step overlapped melting process, which indicates that the compositions diverge away the eutectic composition. The values of T_m, T_g and T_x of the Zr/Nb-based alloys are higher than that of the Zr/Ti-based BMG.[7,8] This is due to the substitution of Nb (with higher melting temperature T_m = 2741 K) for Ti (T_m = 1941 K). The higher value of T_g and T_x may extend the application temperature region of the BMG as engineering materials. Figure 2 presents XRD patterns of the alloys. The XRD patterns of the A3 and B4 alloys [as shown in Figs. 2(e), (f)] show some sharp crystalline peaks superimposed on diffused amorphous peaks indicating the mixture of crystalline and amorphous phases. For the alloy B3 [Fig. 2(d)], XRD pattern shows several small crystalline peaks superimpose on the amorphous diffused peak. The crystalline peaks were identified to be crystalline Zr_2Cu and Zr_2Fe. By reducing Nb content to 8 at% (alloy C1), fully amorphous with diameter of 5 mm is obtained by water quenching as show in [Fig. 2(b)]. The alloy C0 with diameter of 8 mm and alloy B0 with diameter of 3 mm [as shown in Figs. 2(a), (c)] are also fully amorphous phase ascertained by XRD and TEM observation.

To evaluate the GFA of the Zr/Nb based alloys, the $Zr_{45}Nb_{10}Cu_{13}Ni_{10-x}Be_{22-y}Fe_{x+y}$ alloys were quenched using the same cooling rate, the amorphous phase fraction (F_{BMG}) was examined from the DSC curves as follow:[10]

$$F_{BMG} = \frac{\Delta H_P}{\Delta H_T}$$

where ΔH_T is the crystallization enthalpy of the fully amorphous alloy, ΔH_P is the crystallization enthalpy of the various samples cooled at a constant rate.

The changes of the T_m, T_g and T_x with Fe addition of the Zr/Nb-based alloys (10 at%Nb) are plotted in Fig. 3. The change tendency of T_m is similar to that of T_g, and the lowest point of the T_m and T_g is at 8 at%Fe. T_x does not change obviously indicating that the thermal stability is not sensitive to the Fe addition. The changes of the reduced glass transition temperature T_{rg} ($T_{rg} = T_g/T_m$), ΔT and F_{BMG} with different Fe additions are plotted in Fig. 4. It can be clearly seen that the change tendency of ΔT is the same as that of the F_{BMG}, while T_{rg} keeps almost unchanged upon Fe addition. Therefore ΔT is a more suitable parameter for expressing the GFA of the alloy system. The T_{rg} has been successfully used to evaluate the GFA of an alloy. Turnbull[11] suggests that large T_{rg} means excellent GFA, when T_{rg} is larger than 0.67, the nucleation and growth of crystalline phase in supercooled liquid are highly restricted. However, T_{rg} does not characterize the GFA well of the Zr/Nb-based BMGs as shown in Fig. 4. The phenomenon has also been found in other BMG systems.[2,12] So, ΔT can be used to represent GFA for the bulk metallic glass forming alloys. The larger the value of the ΔT, the higher the GFA. This phenomenon may be related to the

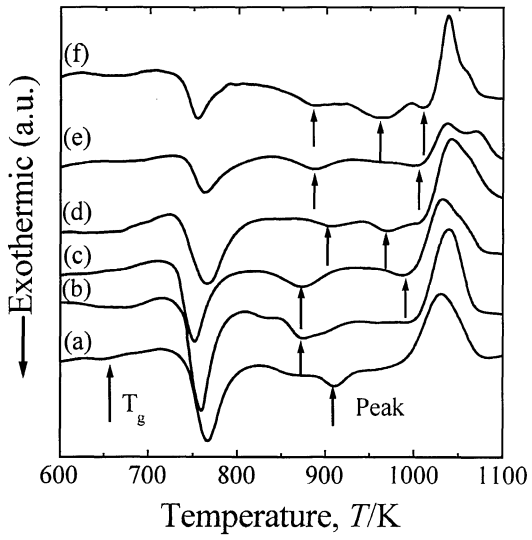

Fig. 1 DTA curves of the Zr/Nb-based alloys at a heating rate of 0.33 K/s, alloy C0 of 8 mm-diameter rod (a), alloy B0 of 3 mm-diameter rod (b), alloy B3 of 8 mm-diameter rod (c), alloy C1 of 5 mm-diameter rod (d), alloy A3 of 8 mm-diameter rod (e), alloy B4 of 8 mm-diameter rod (f).

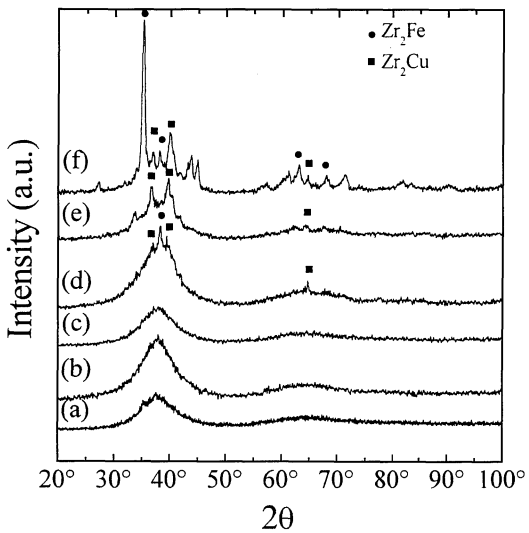

Fig. 2 XRD curves of the Zr/Nb-based alloys, alloy C0 of 8 mm-diameter rod (a), alloy C1 of 5 mm-diameter rod (b), alloy B0 of 3 mm-diameter rod (c), alloy B3 of 8 mm-diameter rod (d), alloy A3 of 8 mm-diameter rod (e), alloy B4 of 8 mm-diameter rod (f).

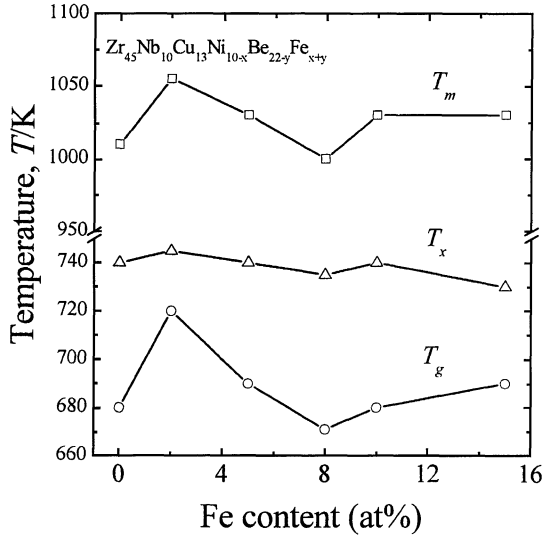

Fig. 3 The change of T_g, T_x and T_m with Fe content in the $Zr_{45}Nb_{10}Cu_{13}Ni_{10-x}Be_{22-y}Fe_{x+y}$ alloys.

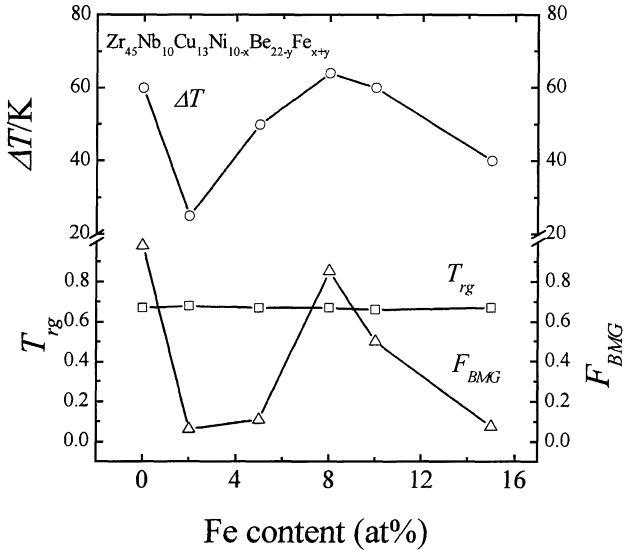

Fig. 4 The change of T_{rg}, ΔT_x and F_{BMG} with the Fe content in the $Zr_{45}Nb_{10}Cu_{13}Ni_{10-x}Be_{22-y}Fe_{x+y}$ alloys.

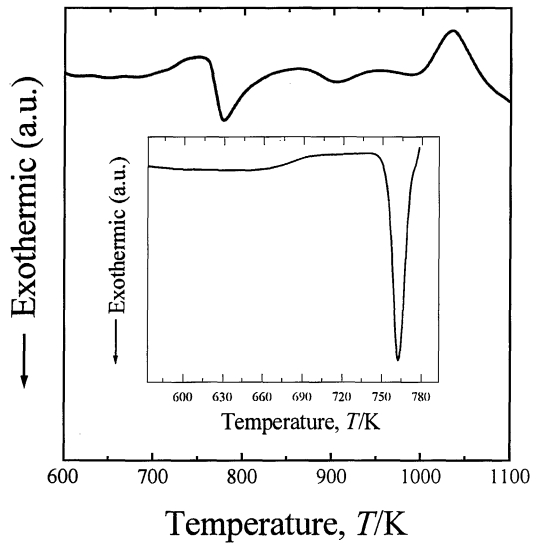

Fig. 5 DTA curve of the $Zr_{48}Nb_8Cu_{12}Fe_8Be_{24}$ alloy with a heating rate of 0.67 K/s. The inset is DSC curve of the $Zr_{48}Nb_8Cu_{12}Fe_8Be_{24}$ alloy with a heating rate of 0.67 K/s.

microstructure difference between the BMG and the conventional metallic glass. The large ΔT of the BMGs originates from their microstructure characteristics. According to conventional nucleation theory, crystallization is determined by the nucleation barrier and atomic diffusion in the supercooled liquid state. Higher nucleation barrier or higher interfacial energy between solid and liquid phases, and lower diffusivity or higher viscosity in the supercooled liquid will suppress the nucleation and growth of the crystalline phases. The more compact microstructure in the melt of the bulk glass forming alloy leads to an increase in interfacial energy and viscosity, and then inhibits the nucleation and growth in the supercooled liquid state.[13] Thus the supercooled liquid of the multicomponent alloy is much more stable against crystallization and has a high resistance to the nucleation and high stability in larger temperature range. ΔT reflects the microstructure characteristics of the BMG. This is the reason why ΔT can characterize the GFA of bulk glass forming alloys.

A series of experimental results indicate that $Zr_{48}Nb_8Cu_{12}Fe_8Be_{24}$ alloy has the best GFA in ZrNbCuFeBe glass forming system. The BMG can be formed in a rod of 8 mm diameter by water quenching method. Figure 5 shows DTA trace of the BMG with a heating rate of 0.67 K/s. A distinct glass transition process signaled by an endothermic change can be observed in the figure, a large exothermic peak at 751 K is corresponding to the crystallization event. There is a large endothermic peak corresponding to the melting process followed the crystallization peak. From the DTA trace, the measured values of T_g, T_x and T_m are much higher than that of the $Zr_{41}Ti_{14}Cu_{12.5}Ni_{10}Be_{22.5}$ alloy.[7,8] The inset of Fig. 5 is DSC trace of the BMG near the SLR with the same heating rate, it shows a wide extended SLR and a sharp crystallization peak. The DTA and DSC curves indicate that the $Zr_{48}Nb_8Cu_{12}Fe_8Be_{24}$ alloy has excellent glass forming ability and higher thermal stability. The isothermal annealing experiments as shown in Fig. 6 also confirm the excellent thermal stability. The figure shows the amorphous state of the alloy does not change up to 673 K, this temperature is a bit larger than the T_g. When the annealing temperature raised to 723 K, crystallization peaks with large full width at half-maximum are observed superimposed on the diffused peak, indicating the precipitation of nano-crystalline phases, the crystalline phase is identified to be Zr_2Fe. When the annealing temperature is larger than the T_x, more unidentified crystalline phases are observed.

The elastic constants (Young' modulus E, shear modulus G, bulk modulus K, and Poison's ratio (μ) and Debye temperature (θ_D) of the Zr/Nb and Zr/Ti-based alloys calculated from the ultrasonic velocities are listed in Table 2. The elastic constants of $Zr_{41}Ti_{14}Cu_{12.5}Ni_{10}Be_{22.5}$ calculated from the ultrasonic methods agree well with the results obtained by other methods.[14] The values of E, G and θ_D of the Zr/Nb-based BMGs are smaller than those of the Zr/Ti-based BMGs, the values of K of the Zr/Nb-based BMGs are close to those

Table 2 Comparison of the Zr/Nb-based alloys with that of the Zr/Ti-based BMGs in elastic and mechanical properties.

Samples	E (GPa)	G (GPa)	K (GPa)	μ	θ_D (K)	ρ (g/cm^3)	K/G	H_V (GPa)
$Zr_{45}Nb_{10}Cu_{13}Ni_{10}Be_{22}$	98.9	36.4	117.9	0.36	308	6.52	3.2	6.32
$Zr_{45}Nb_8Cu_{13}Ni_4Be_{22}Fe_8$	95.5	35.1	114.9	0.36	304	6.54	3.3	6.08
$Zr_{48}Nb_8Cu_{14}Ni_{12}Be_{18}$	93.9	34.3	118.3	0.37	299	6.70	3.5	6.09
$Zr_{45}Nb_{10}Cu_{13}Ni_2Be_{22}Fe_8$	96.8	36.1	100.5	0.34	306	6.60	2.8	7.55
$Zr_{48}Nb_8Cu_{12}Fe_8Be_{24}$	95.7	35.2	113.5	0.36	306	6.44	3.2	5.85
$Zr_{41}Ti_{14}Cu_{12.5}Ni_{10}Be_{22.5}$	101.2	37.4	114.1	0.35	328	6.13	3.1	5.97
$Zr_{41}Ti_{14}Cu_{12.5}Ni_{10}Be_{22.5}C_1$	106.0	39.5	107.3	0.34	335	6.16	2.7	6.13
$Zr_{34}Ti_{15}Cu_{10}Ni_{11}Be_{28}Y_2$	109.8	41.0	113.9	0.34	352	5.78	2.8	6.07

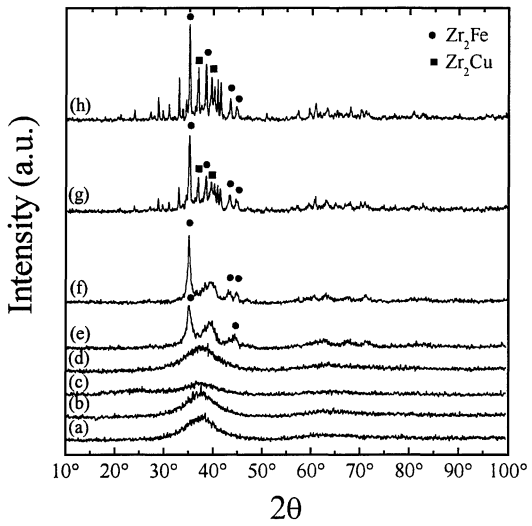

Fig. 6 XRD patterns of the $Zr_{48}Nb_8Cu_{12}Fe_8Be_{24}$ BMG annealed at different temperature for two hours. (a) 523 K; (b) 573 K; (c) 623 K; (d) 673 K; (e) 723 K; (f) 773 K; (g) 823 K; (h) 873 K.

of the Zr/Ti-based BMGs, while K/G and ρ of the Zr/Nb-based BMGs are higher compared to Zr/Ti based BMGs, the higher value of K/G and μ may indicates higher plastic deformation ability.[15] The alloy B3 has the highest value of H_V, which is attribute to the mixture structure of crystalline and amorphous phases [Fig. 2(d)]. The ultrasonic study indicates that the Zr/Nb-based BMG, like Zr/Ti-based BMG, has excellent elastic and mechanical properties, and the elastic and mechanical properties of the BMG are not sensitive to the Fe addition.

4. Conclusions

The Zr/Nb-based BMGs with excellent glass forming ability, elastic and mechanical properties are obtained by water quenching method. The GFA of the alloys is sensitive to the Fe addition, and the highest GFA is achieved at 8 at% of Fe addition. The $Zr_{48}Nb_8Cu_{12}Fe_8Be_{24}$ alloy is found to have the best GFA in the ZrNbCuFeBe glass forming system. ΔT is more effective than T_{rg} to evaluate the GFA of the Zr/Nb-based alloys. Comparing with the Zr/Ti-based BMG, the Zr/Nb-based BMGs have higher thermal stability, and higher glass transition temperature. The Zr/Nb-based BMG, like Zr/Ti-based BMG, has excellent elastic and mechanical properties

Acknowledgement

The authors are grateful for the financial support of the National Natural Science Foundation of China. (Granted numbers: 59925101, 59871059 and 19874075)

REFERENCES

1) A. L. Greer: Nature, **366** (1993), 303–304.
2) A. Inoue: Mater. Trans., JIM, **36** (1995), 866–875.
3) A. Peker and W. L. Johnson: Appl. Phys. Lett., **63** (1993), 2342–2344.
4) J. Eckert: Mater. Sci. Forum, **312–314** (1999), 3–12.
5) W. Liu, W. L. Johnson, S. Schneider, U. Geyer and P. Thiyagarajan: Phys. Rev. B **59** (1999), 11755–11759.
6) W. Klement, R. Willens and P. Duwez: Nature (London), **187** (1960), 869.
7) W. H. Wang and H. Y. Bai: J. Appl. Phys., **84** (1998), 5961–5968.
8) D. Q. Zhao, Y. X. Zhuang, Y. Zhang and W. H. Wang: *Acta Metallurgica Sinica*, **36** (2000), 329–333 (in chinese).
9) Y. Zhang, D. Q. Zhao, Y. X. Zhuang, M. X. Pan and W. H. Wang: *Acta photonica Sinica*, **28** (Z2) (1999), 35–38 (in chinese).
10) C. Fan, A. Takeuchi and A. Inoue: Mater. Trans., JIM, **40** (1999), 42–51.
11) D. Turnbull: Contemporary Phys., **10** (1969), 473.
12) Y. Li, S. C. Ng, C. K. Ong, H. H. Hng and T. T. Goh: *Scripta Mater.*, **36** (1997), 783–787.
13) W. H. Wang, Q. Wei and H. Friedrich: Phys. Rev. B, **57** (1998), 8211–8217.
14) R. D. Conner, R. B. Dandliker and W. L. Johnson: *Acta Mater.*, **46** (1998), 6089–6102.
15) W. H. Wang, R. J. Wang, F. Y. Li, D. Q. Zhao and M. X. Pan: Appl. Phys. Lett., **74** (1999), 1803–1805.